arXiv:1602.01477v2 [cond-mat.mes-hall] 30 Aug 2016

Designing Quantum Spin-Orbital Liquids in Artificial Mott Insulators

Xu Dou,[1] Valeri N. Kotov,[2] and Bruno Uchoa[3]

[1]*Department of Physics and Astronomy, University of Oklahoma, Norman, OK 73069, USA*
[2]*Department of Physics, University of Vermont, Burlington, VT 05405, USA*
[3]*Department of Physics and Astronomy, University of Oklahoma, Norman, OK 73069, USA*

(Dated: August 31, 2016)

Quantum spin-orbital liquids are elusive strongly correlated states of matter that emerge from quantum frustration between spin and orbital degrees of freedom. A promising route towards the observation of those states is the creation of artificial Mott insulators where antiferromagnetic correlations between spins and orbitals can be designed. We show that Coulomb impurity lattices on the surface of gapped honeycomb substrates, such as graphene on SiC, can be used to simulate SU(4) symmetric spin-orbital lattice models. We exploit the property that massive Dirac fermions form mid-gap bound states with spin and valley degeneracies in the vicinity of a Coulomb impurity. Due to electronic repulsion, the antiferromagnetic correlations of the impurity lattice are driven by a super-exchange interaction with SU(4) symmetry, which emerges from the bound states degeneracy at quarter filling. We propose that quantum spin-orbital liquids can be engineered in artificially designed solid-state systems at vastly higher temperatures than achievable in optical lattices with cold atoms. We discuss the experimental setup and possible scenarios for candidate quantum spin-liquids in Coulomb impurity lattices of various geometries.

Quantum spin liquids are highly entangled states that can emerge in antiferromagnetic lattices in the presence spin degeneracies and frustration. Spin-orbital liquids result from systems that have not only spin degeneracies but also orbital degeneracies [1, 2]. Those states are strongly correlated, have non-local excitations, but nevertheless do not break any symmetries. In spite of mounting theoretical effort [3–7], a significant difficulty in finding viable candidates for quantum spin-orbital liquids is the fact that normally the interactions governing spin and orbital degrees of freedom have very different energy scales [8–10]. Consequently those degrees of freedom are decoupled at sufficiently low temperatures, hindering the quantum frustration that is required to entangle orbitals and spins. Very recently, x-ray scattering studies in magnetic honeycomb based $BaCuSb_2O_9$ crystals reported indications of spin-orbital entanglement at low temperature [11, 12].

An alternative to identifying crystals where spins and orbtitals are strongly coupled would be instead to create artificial crystals where spin and orbital quantum numbers become interchangeable. Such property appears in magnetic Hamiltonians that display SU(4) symmetry [13]. Recent experiments with cold atoms reported spectroscopic quantum simulations in small artificial magnetic systems with SU($N \leq 10$) symmetry at ultra low temperature [14, 15]. Mott physics with SU(2) spins has been observed in optical lattices with ultra cold atoms inside a parabolic potential [16]. In those systems, strong correlations emerge only at extremely low temperatures, making a possible detection of quantum spin-liquids challenging [17]. Solid-state systems where antiferromagnetic interactions have SU(4) symmetry are not common, since in real materials, anisotropies and off-diagonal hopping matrix elements in the degenerate orbital space usually lower that symmetry [18].

We propose a solid-state system that can be experimentally designed with scanning tunneling microscopy (STM) tips by positioning Coulomb impurity adatoms in a periodic array on top of an insulating honeycomb substrate. The electrons in those substrates can be described by massive Dirac fermions, which form bound states around the impurities [19–21]. Those bound states have spin and valley degeneracies, which are dual to spin-orbital degrees of freedom. We theoretically construct an artificial lattice where each impurity site is quarter filled with valley and spin polarized states. The problem has an emergent SU(4) symmetry that follows from the orthogonality between the two different valley spaces. In systems like graphene, SU(4) symmetry is known to emerge in the quantum Hall regime [22]. Electronic interactions lead to a variety of broken symmetry states in both spins and valleys [23–28].

The spin-orbital exchange interactions are calculated in three different impurity lattice geometries: triangular, square and honeycomb, shown in Fig. 1. We find the constraints on the impurity lattice in the regimes where the system is expected to behave as a Mott insulator dominated by antiferromagnetic interactions between sites. We propose the experimental conditions for the observation of those states. For honeycomb substrates such as graphene grown on SiC [29, 30], we show that the Mott regime of entangled spins and orbitals is experimentally accessible and that the superexchange interaction can be as large as $J_s/k \sim 60 - 120$ K. The experimental signatures of strongly correlated states are discussed based on possible scenarios predicted for SU(4) spin-orbital models [31–34], including quantum spin-orbital liquids.

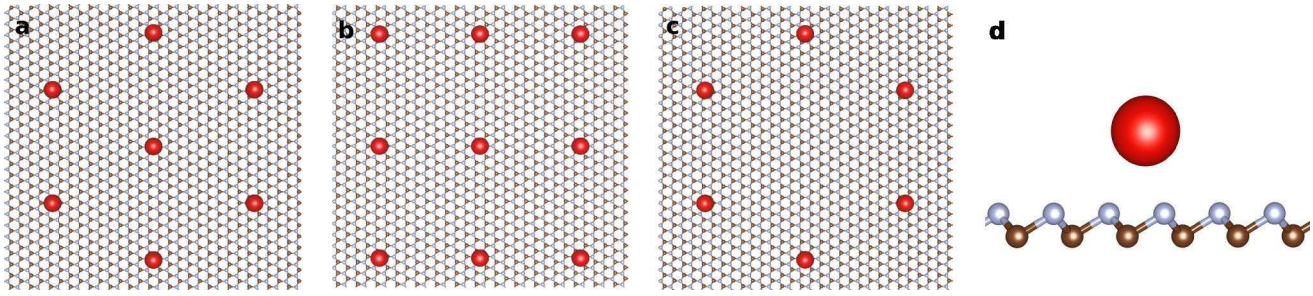

Figure 1: **Coulomb impurity lattices.** Honeycomb substrate with unequal sublattices decorated with a superlattice of charged impurities. In the three configurations, triangular (a), square (b) and honeycomb (c), the impurities are separated by a superlattice constant L, and sit at a distance d away from the plane of the substrate (d). All impurities interact with electrons via Coulomb, $1/r$ potential.

Results

Coulomb impurity problem. The wavefunction of the Coulomb impurity bound states for 2D massive Dirac fermions, $\Psi(\mathbf{r})$, can be derived from the Dirac equation

$$(-i\hbar v\boldsymbol{\sigma}\cdot\boldsymbol{\nabla}+V(r)+mv^2\sigma_z)\Psi(\mathbf{r})=\epsilon\Psi(\mathbf{r}). \quad (1)$$

$\boldsymbol{\sigma}=(\sigma_x,\sigma_y)$ is a vector with off-diagonal Pauli matrices, σ_z is the diagonal Pauli matrix, v is the Fermi velocity and m is the mass term of the substrate, that describes a gap in the electronic spectrum, $\Delta=2mv^2$. $V(r)=-Ze^2/\kappa\sqrt{r^2+d^2}$ is the Coulomb impurity potential, where is Z the atomic number of the impurity, e is the electron charge, κ the dielectric constant of the surface, and $d\approx 2-3$Å is the out-of-plane distance between the impurity and the plane of the substrate.

The impurity potential decays as $V(r)\sim 1/r$ in the $r\gg d$ limit and saturates into a constant in the opposite limit. The potential can be written as

$$V(r)=-Z\frac{e^2}{\kappa}\left[\frac{1}{r}\theta(r-a)+\frac{1}{a}\theta(a-r)\right] \quad (2)$$

where a is an effective real space cut-off which regularizes the Coulomb potential. The size of the cut-off can be chosen as $a\sim d$ and is typically of the order of the impurity size. This regularization procedure is well known in quantum electrodynamics in 3+1 dimensions (QED_{3+1}) and has been successfully used to explain the experimentally observed dive of bound states in the lower continuum around super-heavy nuclei with atomic number $Z>137$ [35, 36]. Both in QED_{3+1} as in the 2D case, the wavefunction of the Coulomb impurity bound states decay over a characteristic distance defined by the Compton wavelength $\lambda_C=\hbar/mv$.

In cylindrical coordinates, the solution of Eq. (1) is in the form

$$\Psi(r,\phi)=\frac{c}{\sqrt{2\pi}}\begin{pmatrix}F_j^{(-)}(r)\mathrm{e}^{i(j-\frac{1}{2})\phi}\\ iF_j^{(+)}(r)e^{i(j+\frac{1}{2})\phi}\end{pmatrix}, \quad (3)$$

where $j=\pm\frac{1}{2},\pm\frac{3}{2}\ldots,m+\frac{1}{2}$ ($m\in\mathbb{Z}$) are the possible angular momentum states, and c is the normalization constant. The energy spectrum is quantized by the usual quantum numbers in the Hydrogen atom problem, $n\in\mathbb{N}$ and j [19–21]. The degeneracy of the $\pm|j|$ angular momenta states for a given $n>0$ however is lifted. At $n=0$, only the $j=\frac{1}{2}$ state is allowed.

Defining the impurity strength by the dimensionless coupling $g\equiv Z\alpha$, where $\alpha=e^2/\kappa\hbar v$ is the screened fine structure constant of the substrate, there are two known regimes of the problem: the perturbative regime $g\ll 1$, where the bound states are shallow, and the strong coupling regime $g\gtrsim 0.5$, where they dive in the negative sector of the energy spectrum, as shown in Fig. 2. At fixed g, the lowest energy level is the $n=0$, $j=\frac{1}{2}$ state, followed by the first excited state $n=1$, $j=-\frac{1}{2}$. There is an infinite number of higher excited states inside the gap Δ. The latter states have very small binding energies and are not relevant to this discussion.

We are interested in the strong coupling regime of the problem ($g\gtrsim 0.5$), where the confining potential is deep and the energy separation between the ground state level and the first excited state is of the order of $\sim\Delta/2$. At sufficiently large coupling, $g>g_c$, the lowest energy state level dives in the continuum of negative energy states outside of the gap. This regime is known as the supercritical regime. At the critical one, when $g=g_c$ the energy of the lowest level is exactly at the edge of the gap, $\epsilon=-mv^2$. In the subcritical regime, $0.5\lesssim g<g_c$, which is the focus of this paper, the levels are strongly localized and sharply defined inside the gap. For a Coulomb impurity on top of graphene epitaxially grown on SiC, where $\Delta\sim 0.26$ eV [29], and for a typical small distance cut-off $a\approx 2.8$Å, $g_c=0.916$. In general, the critical coupling $g_c\sim 1$. The energy of the levels follows directly from matching the wave function at $r=a$, similarly to the procedure in the QED_{3+1} case. The solution of the subcritical regime can be calculated either numerically [19] or for the purposes of this work, analytically, as detailed in the Supplemental Materials.

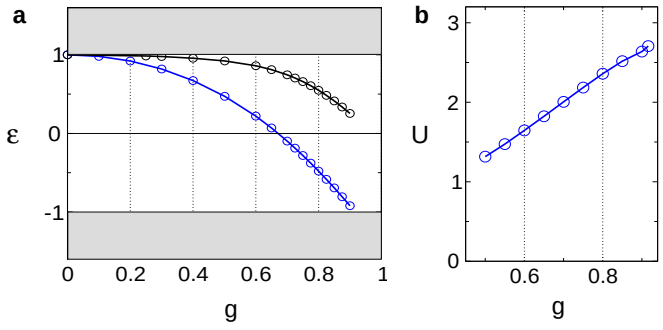

Figure 2: **Single impurity energy scales.** (a) Energy of the Coulomb impurity bound states ϵ, in units of $mv^2 = 0.13$ eV, as a function of the dimensionless coupling $g = Z\alpha$. Blue dots: ground state level, $n = 0$, $j = \frac{1}{2}$. Black dots: first excited state, $n = 1$, $j = -\frac{1}{2}$. At $g = g_c \approx 0.916$, the lowest energy level dives in the continuum of negative energy states at $\epsilon = -mv^2$. In the subcritical regime $g \lesssim g_c$, the two levels have an energy separation $\sim mv^2$. (b) Hubbard U, in units of $mv^2\alpha$, versus g in the strong coupling regime $0.5 \leq g \leq g_c$. U is comparable to the energy of the gap $\Delta = 2mv^2$.

Impurity lattice model. In a honeycomb lattice with massive Dirac fermions, the quasiparticles also have two valley flavors, in addition to the spin. The Coulomb impurity bound states therefore must have both spin and valley degrees of freedom. The Dirac equation in this case is

$$\begin{pmatrix} \hat{\mathcal{H}}_+(\mathbf{r}) & 0 \\ 0 & \hat{\mathcal{H}}_-(\mathbf{r}) \end{pmatrix} \Phi(\mathbf{r}) = \epsilon \Phi(\mathbf{r}), \tag{4}$$

where $\hat{\mathcal{H}}_+(\mathbf{r}) = -i\hbar v \boldsymbol{\sigma} \cdot \boldsymbol{\nabla} + V(r) + mv^2\sigma_z$ is the Dirac Hamiltonian matrix in valley $+$ and $\hat{\mathcal{H}}_-(\mathbf{r}) = \hat{\mathcal{H}}_+^*(\mathbf{r})$ in the opposite valley. The eigenvectors are the four component spinors $\Phi_{j,+}(\mathbf{r}) = (\Psi_j(\mathbf{r}), \mathbf{0})$ and $\Phi_{j,-}(\mathbf{r}) = (\mathbf{0}, \Psi_j^*(\mathbf{r}))$, which are degenerate. The j-th energy level is four-fold degenerate, with two spins and two valleys. The valleys describe the orbital motion of an electron around a Coulomb impurity. They effectively behave as a pseudo-spin with SU(2) symmetry, as the actual spins.

Once Coulomb interactions among the electrons in the bound state are included, those states tend to spin and valley polarize due to correlations and Pauli blocking. In the ground state, $j = \frac{1}{2}$, the Coulomb interaction can be expressed in terms of a Hubbard U term

$$\mathcal{H}_U = \frac{1}{2} U \sum_{\{\nu\},\{\sigma\}} \hat{n}_{\nu,\sigma} \hat{n}_{\nu',\sigma'} (1 - \delta_{\nu,\nu'}\delta_{\sigma\sigma'}), \tag{5}$$

where

$$U = \int \mathrm{d}^2 r \mathrm{d}^2 r' |\Phi_{\frac{1}{2},\nu}(\mathbf{r})|^2 \frac{e^2}{\kappa|\mathbf{r} - \mathbf{r}'|} |\Phi_{\frac{1}{2},\nu'}(\mathbf{r}')|^2 \tag{6}$$

is a valley independent local repulsion. $\hat{n}_{\nu,\sigma} = c_{\nu,\sigma}^\dagger c_{\nu\sigma}$ is the number operator per valley and spin at the bound state, where $c_{\nu,\sigma}$ annihilates one electron in the $j = \frac{1}{2}$ level on valley ν with spin σ. Due to the orthogonality of the eigenspinors, $\Phi_{j,+}^\dagger(\mathbf{r})\Phi_{j,-}(\mathbf{r}) = 0$, the exchange interaction between electrons in different valleys around the same Coulomb impurity is zero.

In Fig. 2, we calculate U as a function of the dimensionless impurity coupling g in the strong coupling regime $0.5 \lesssim g < g_c$. At $g = g_c$, $U = 2.7\, mv^2\alpha$, dropping to $U = 1.35\, mv^2\alpha$ at $g = 0.5$. When U is large and only the $j = \frac{1}{2}$ level is filled, the ground state will be singly occupied in one of the four possible states: $|\bullet\rangle = |+,\uparrow\rangle$, $|\bullet\rangle = |+,\downarrow\rangle$, $|\bullet\rangle = |-,\uparrow\rangle$, and $|\bullet\rangle = |-,\downarrow\rangle$.

We would like to write down an effective lattice model for a strongly correlated lattice of Coulomb impurities, each one having a quarter filled bound state in one of the four possible states above. Those electrons can hop between different Coulomb impurity sites, with each one having a Hubbard U energy, that penalizes multiply occupied sites, and also having a well defined valley and spin. The hopping term is

$$\mathcal{H}_t = -t \sum_{\langle ij \rangle} \sum_{\nu,\sigma} c_{i,\nu,\sigma}^\dagger c_{j,\nu,\sigma}, \tag{7}$$

with c_i describing the annihilation operator of an electron in the $j = \frac{1}{2}$ level siting on an impurity site located at $\mathbf{R}_i$, and $\langle ij \rangle$ denotes summation over nearest neighbor (NN) sites. The hopping parameter of the Coulomb impurity lattice is

$$t_{ij} = \int \mathrm{d}^2 r \Phi_{\frac{1}{2},\nu}^\dagger(\mathbf{r}_i) \sum_{k \neq i} V(|\mathbf{r}_k|) \Phi_{\frac{1}{2},\nu}(\mathbf{r}_j) \tag{8}$$

where $\mathbf{r}_i \equiv \mathbf{r} - \mathbf{R}_i$ is the position relative to site i. Hopping between Coulomb impurity sites conserves valley due to the orthogonality of eigenspinors in the valley space, $\Phi_{\frac{1}{2},+}^\dagger(\mathbf{r}_i)\Phi_{\frac{1}{2},-}(\mathbf{r}_j) = 0$. Because of the summation of the potential over lattice sites and the long range nature of the Coulomb interaction, the value of t is influenced by the geometry of the lattice.

In the limit $U \gg t$, we can expand the effective Hamiltonian in second order perturbation theory in the hopping, $\mathcal{H}_s = -\mathcal{H}_t \mathcal{H}_U^{-1} \mathcal{H}_t + \mathcal{O}(t^4)$. The Hamiltonian that results is the superexchange interaction, which favors antiferromagnetic alignment of spins or valleys. This interaction is of order $J_s = t^2/U$ and lowers the energy cost for electrons to hop back and forth between two NN sites. The superexchange competes with the exchange interaction between NN sites, which is ferromagnetic and defined by $J_{e,ij} = -\frac{1}{2} \int \mathrm{d}^2 r \mathrm{d}^2 r'\, \Phi_{\frac{1}{2},\nu}^\dagger(\mathbf{r}_i)\Phi_{\frac{1}{2},\nu}(\mathbf{r}_j) \frac{e^2}{\kappa|\mathbf{r}-\mathbf{r}'|} \Phi_{\frac{1}{2},\nu'}^\dagger(\mathbf{r}_j')\Phi_{\frac{1}{2},\nu'}(\mathbf{r}_i')$, with $J_{e,\langle ij \rangle} \equiv J_e < 0$. As shown in the Methods section, both the superexchange and the exchange interactions map into a Kugel-Khomskii type Hamiltonian [37] with

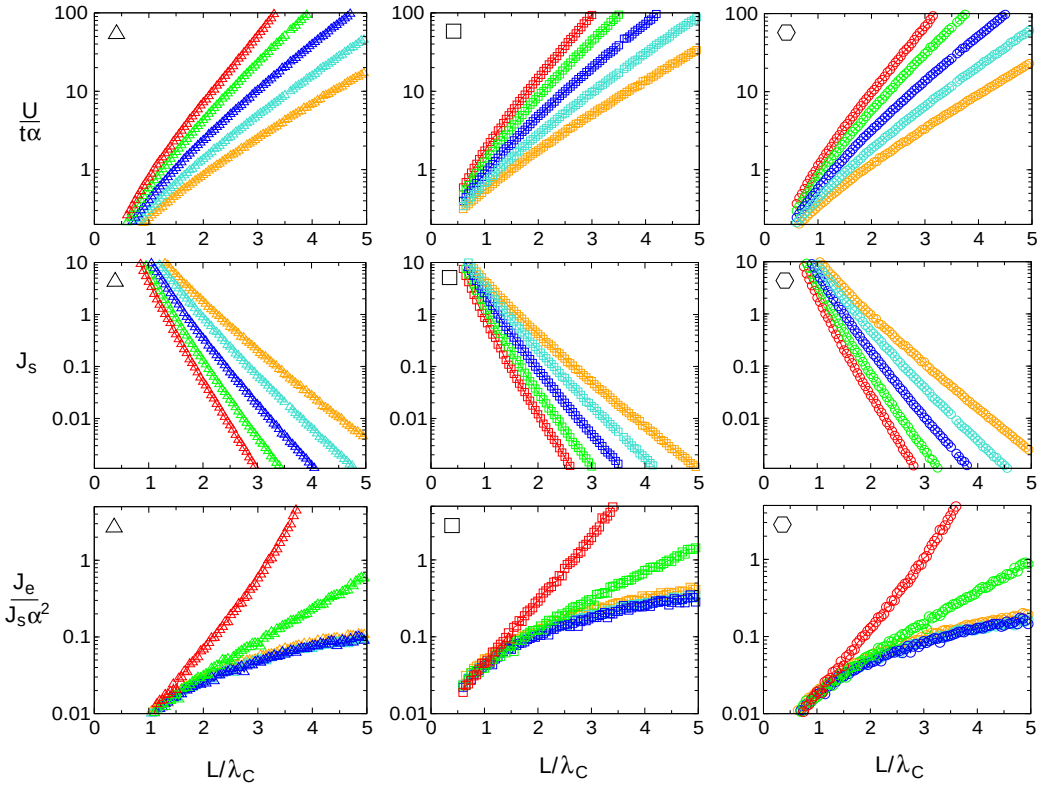

Figure 3: **Correlations in Coulomb impurity lattices.** Left column (△): triangular lattice; middle column (□) square lattice; right column (⬡): honeycomb lattice. Red dots: $g = 0.9$; green: $g = 0.8$; blue: $g = 0.7$; cyan: $g = 0.6$; orange: $g = 0.5$. Top row: ratio between the onsite repulsion (U) and the kinetic energy (t) times the fine structure α versus the superlattice constant L normalized by the Compton wavelength $\lambda_C = \hbar/mv$. For a substrate with a gap of of $\Delta = 0.26$ eV (graphene on SiC), $\lambda_C \approx 46$Å. When $U/t \gtrsim 5$, the system is strongly correlated: the Coulomb impurities form a lattice of local spin-orbitals. Middle row: Superexchange interaction, $J_s = t^2/U$ in units of mv^2/α, versus L/λ_C. Bottom row: ratio between the exchange interaction J_e and the superexchange interaction J_s times α^2.

exact SU(4) symmetry,

$$\mathcal{H} = J \sum_{\langle ij \rangle} \left(\frac{1}{2} + 2\boldsymbol{\tau}_i \cdot \boldsymbol{\tau}_j \right) \left(\frac{1}{2} + 2\mathbf{S}_i \cdot \mathbf{S}_j \right), \qquad (9)$$

where $\boldsymbol{\tau}_i$ is the valley pseudospin operator and $\mathbf{S}_i$ the spin operator on a given site. Hamiltonian (9) is symmetric under any permutation among the four different valley-spin flavors (colors).

The coupling $J \sim J_s > 0$ in the regime where the superexchange coupling dominates ($t^2/U \gg J_e$). The superexchange interaction is antiferromagnetic, and can drive the spin-orbital lattice into frustrated phases where no symmetry is broken. In the opposite regime ($J_e \gg t^2/U$), the coupling $J = -J_e < 0$ changes sign, and the system tends to order in a ferromagnetic state at zero temperature.

Numerical results. In Fig. 3 we show the ratio of $U/t\alpha$ as a function of the impurity lattice constant L for three different geometries: triangular (△), square (□) and honeycomb (⬡). L is normalized by the Compton wavelength λ_C, which is inversely proportional to the mass gap of the substrate. In the regime where $U/t \gtrsim 5$, the system is a strongly correlated insulator and can be effectively described as a lattice of local valley-orbitals and spins. The different curves in each panel correspond to different impurity couplings, with g ranging from 0.5 to the critical value $g_c \sim 0.916$. At the middle row panels, we display the superexchange coupling J_s (in units of mv^2/α) as a function of L. For couplings $g < g_c$, when $U/t\alpha \sim 12$ the superexchange coupling ranges from $J_s\alpha/mv^2 \approx 0.01 - 0.02$ for g running between 0.5 and 0.9 in all geometries we tested, as indicated in Fig. 3. In the regime $U/t\alpha \sim 20$, the super exchange is in the range $J_s\alpha/mv^2 \approx 0.003 - 0.007$.

For graphene on SiC substrate with $\Delta = 2mv^2 \sim 0.26$ eV, the Compton wavelength $\lambda_C \approx 46$Å. On the surface of SiC ($\kappa \sim 5.2$) the fine structure constant $\alpha \approx 0.42$. The size of the superlattice constant L that corresponds to a fixed value of J_s varies slightly depending on the geometry of the lattice. At $g \approx g_c$ (red dots), the impurity valence $Z \sim 2$. When $U/t\alpha = 12$ ($U/t \approx 5$), the superexchange interaction between NN sites is $J_s/k \sim 59$ K and corresponds to impurity lattice constants $L/\lambda_C \approx 2.25$ (△), 1.9 (□), and 2.1 (⬡), resulting in $L \sim 90 - 100$Å.

At $g = 0.5$ or $Z \sim 1$ (orange dots), the wavefunctions are more weakly bounded to the impurities and hence more extended. The same ratio of $U/t \approx 5$ corresponds to $J_s/k \sim 28$ K and larger superlattice constants $L/\lambda_C \sim 4.6\,(\triangle)$, $3.9\,(\square)$, and $4.3\,(\bigcirc)$, respectively, with $L \sim 180\text{Å}-200\text{Å}$. For a larger gap of $\Delta \sim 0.5$ eV [30], the superexchange nearly doubles ($J_s \sim 56 - 118$ K) while the Compton wavelength is halved. When $U/t\alpha = 20$ ($U/t \approx 8.5$), $J_s/k \sim 10 - 20$ K.

In the regime of interest, where U/t is large, U is the largest energy scale in the problem. The superexchange interaction competes with the exchange one J_e and, in principle, both can be of the same order. In the bottom row of the panels in Fig. 3 we plot the ratio between $J_e/J_s\alpha^2$. For $\alpha < 1$, the superexchange interaction clearly dominates the exchange interaction, and is at least three times larger for $U/t\alpha \lesssim 20$. When considering Coulomb impurities on graphene-SiC substrates, where $\alpha = 0.42$, the ratio $J_e/J_s < 0.07$ in all geometries considered in the range $U/t \lesssim 8.5$. The dominant interactions are therefore clearly antiferromagnetic. Due to the SU(4) symmetry, valley and spin degrees of freedom are strongly entangled and may give rise to a spin-orbital liquid in the Mott insulator regime.

Experimental setup. The lattice of Coulomb impurities can be experimentally created with STM tips, which can drag atoms on a surface with atomic precision [38]. Possible substrates include graphene epitaxially grown on SiC, which was shown to develop a gap ranging from $\Delta = 0.26 - 0.5$ eV [29, 30]. In high quality samples, the Fermi level was observed in the middle of the gap [30]. Other crystals, such as MoS_2, $MoSe_2$, and other dichalcogenides [39], have even larger gaps, however they also exhibit large spin-orbit couplings [40], which will lift the SU(4) symmetry of the problem, lowering it to SU(2). Strong unitary disorder connects the two valleys and can also have a similar effect. Disorder effects, however, can be inhibited by properly annealing the substrate.

Among alkaline metals, potassium adatoms ($Z = 1$) are known to spontaneously form two dimensional crystals on honeycomb substrates such as graphite [41]. Higher valence cobalt adatoms have already been studied with STM on graphene and are also possible candidates [42]. The strong coupling regime, where the bound states are deep and well separated, is experimentally accessible for impurities with a valence $Z \sim 1$. That contrasts with the standard relativistic scenario, where the strong coupling regime can be achieved only when the valence is of the order of the inverse of the QED fine structure constant $Z \sim 1/\alpha_{QED} = 137$.

The determination of the impurity lattice constant L that is required to create a Mott insulator with strong antiferromagnetic correlations can be achieved with local spectroscopy measurements around a single impurity. Those measurements can accurately determine the energy of the bound states inside the gap. With the theoretical wavefunctions, one can extract the effective impurity coupling g by comparing the measurement of the energy levels with the calculated result, as shown in Fig. 2. The appropriate range for the impurity lattice constant is indicated in the plots of Fig. 3. Integration of the measured local density of states over the area around the impurity gives the occupation of the ground energy level inside the gap. When the impurity lattice is in the Mott regime, each four-fold degenerate impurity level will remain singly occupied (quarter filling).

Discussion

Recent numerical evidence [31] suggests that the ground state of the antiferromagnetic Hamiltonian (9) in the honeycomb lattice is a strongly correlated state that preserves all the symmetries of the system. This state is a quantum spin-orbital liquid schematically drawn in the left panel of Fig. 4. Every site has a well defined spin-valley state (color) among the four possible colors. Each color has the same neighbors up to color permutations. The pattern preserves both the lattice symmetry and the SU(4) color symmetry.

Color-color correlations appear to decay as a power law, indicating a gapless state, or equivalently, an algebraic quantum spin-orbital liquid with no true long range order. Algebraic spin liquids are generally known to be robust two-dimensional interacting critical states, relevant to a variety of correlated physical models [43]. After comparison of the energy of several different states, the quarter filled π-flux state currently appears as the leading candidate [31]. In the honeycomb lattice, a π-flux in the honeycomb plaquette creates Dirac fermions at quarter filling, which is the regime of interest for Mott insulators with SU(4) symmetry. Those Dirac fermions are (color) spinon excitations, which are four-fold degenerate due to the color symmetry.

Low-energy characteristic probes amenable to 2D systems have been proposed, such as injecting a spin current into the insulator and monitoring the spin bias dependence of the current [45, 46]. In the simplest experimental setup with a single metal-insulator interface, spin accumulation is achieved via the spin Hall effect. In the four-terminal setup, the spin-liquid insulator is coupled to left and right metal leads. Spin current detection occurs through the reverse spin Hall effect in one of the metallic contacts.

In the spin-orbital (valley) case at hand, the spin degrees of freedom in the insulator and in the metal are coupled at the interface. The valleys are decoupled from the orbital degrees of freedom in the metal. Hence the valleys do not experience flips due to the spin current injection. The result is the propagation of a pure spin current with additional valley degeneracy. Consequently, in this case, the spin current will scale in the same way

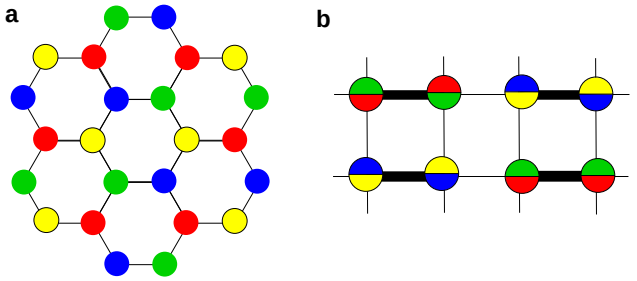

Figure 4: **Spin-orbital color states.** (a) Possible algebraic quantum spin-orbital liquid for the honeycomb lattice in the SU(4) Heisenberg model, numerically predicted in Ref. [31]. This state may correspond to a quarter filled π-flux phase. Each color is surrounded by the same states, up to color permutations. Both crystalline and SU(4) symmetries are intact. (b) Possible dimerized state in the square lattice, with alternating singlets of two colors (after Ref. [33].) This state has long range order and breaks both lattice and color symmetry.

with the bias voltage as in pure spin models. For the π-flux state, the Dirac cone of the spinons is degenerate in all quantum numbers (spin and valley). The spin current scales with the fifth power of the bias voltage, $I_s \sim V^5$ [45, 46]. This result appears to be a universal signature of both spin and spin-orbital liquid phases with gapless Dirac fermion spinons. In general, the power of the spin voltage dependence is sensitive to the nature and dispersion of the spinon excitations. The exact nature of the spin-orbital liquid state in the honeycomb lattice requires further investigation. Nevertheless, the prospects of observing a true quantum spin-orbital liquid in this geometry seem quite promising.

Triangular lattices are natural candidates for quantum disordered states due to their strongly frustrated nature. It was proposed at first that their ground state has plaquette order [13], with plaquettes formed by SU(4) singlets. However more recent work [32] found strong local resonances between plaquette configurations. While more complicated orders with large unit cells can not be ruled out, the ground state appears to be a spin-orbital liquid with no plaquette order. The presence of next-nearest neighbor superexchange J_s' drives the system into magnetically long range ordered state via a quantum phase transition at a critical value $J_s'/J_s \approx 0.12$ [32]. In the proposed Coulomb impurity lattice, we find that ratio to be $\sim 10^{-2}$. On the basis of the existing knowledge about the model, we conclude that a spin-orbital liquid state can be realized in the Mott regime. The nature of this state is not yet known.

There have been suggestions of a variety of different ground states for Hamiltonian (9) in the square lattice. Possibilities include a gapless spin liquid with nodal fermions [34], and a plaquette state [13, 47]. A more recent numerical work has laid more concrete evidence towards a dimerized state depicted in Fig. 4, which breaks both lattice and color symmetry [33]. The thick bonds represent strong bonds, while the think lines are weaker. This particular state has two sets of dimers with two colors each, which alternate along the two main directions of the lattice. Because of the broken symmetry, the elementary excitations are Goldstone modes in the form of gapless (color) magnons. These could also lead to characteristic power law dependencies in the spin current as a function of spin bias [45, 46], with the power being generally smaller than for gapless Dirac spinons (π-flux phase).

Coulomb impurity lattices offer wide possibilities for different frustrated scenarios due to the inherent flexibility in their design. Recent experiments observed evidence for a spin-liquid ground state in the antiferromagnetic Kagome lattice [48]. We conjecture that gapped honeycomb substrates with large spin orbit coupling, such as MoS_2 [40], could be experimentally used to design frustrated artificial Coulomb impurity lattices where the spin degeneracy is explicitly lifted, leaving a pure quantum orbital (valley) liquid in the ground state. The tendency towards frustration is not the unique scenario for artificial lattices supported on gapped honeycomb substrates. For instance, color ferromagnetism is possible in superlattices of mass defects forming quantum rings [49].

In summary, we have shown that Mott insulators having spin and orbital degeneracies can be artificially designed in a solid state system. The emergent SU(4) symmetry of the problem follows from the unique nature of the valley degrees of freedom in honeycomb substrates and does not require fine tuning. We have predicted the conditions for Coulomb impurity lattices to be in the Mott regime and discussed experiments that could detect quantum spin-orbital liquid states.

Most of the current efforts to simulate quantum spin liquids are concentrated in cold atom systems, where the Mott physics is present only at ultra low temperatures [16, 17]. This proposal may lead to significant advances in the experimental design and observation of quantum spin-orbital liquids in solid-state settings.

Methods

Wavefunctions. We assume a real space cut-off for the Coulomb interaction $a = \lambda_C/18$. For a typical mass gap energy $mv^2 \approx 0.13$ eV and $\hbar v \approx 6$eVÅ, as in graphene on SiC, the Compton wavelength $\lambda_C \sim 50$Å, which corresponds to $a \approx 2.8$Å. This number agrees with the typical size of many Coulomb impurities, including alkaline metals.

The analytical form of the 2D Coulomb impurity wavefunctions in the weak coupling regime ($g \ll 1$) is well known [20, 21]. In that regime the cutoff does not play an important role (can be set to zero) and the bound states are shallow. The wavefunctions in the subcritical

strong coupling regime ($0.5 \lesssim g < g_c$) can be solved analytically as well. They correspond to the solution of the Dirac equation in the potential (2) and bare strong similarity to the 3D Dirac equation (QED_{3+1}) case [35, 36].

Setting $\hbar = v = 1$, for $r > a$, the strong coupling solution in the subcritical regime has spinor component amplitudes [**?**]

$$F_j^{(\pm)}(r) = \sqrt{m \mp \epsilon}\, e^{-\rho/2}\rho^{-\gamma-1/2}\frac{\Gamma(2s\gamma)}{\Gamma(s\gamma-\tilde{\epsilon})}G^{(\pm)}(r), \tag{10}$$

where $\gamma = \sqrt{j^2 - g^2}$, $\beta = \sqrt{m^2 - \epsilon^2}$, $\Gamma(x)$ is a gamma function and

$$G^{(\pm)}(r) \equiv \sum_{s=\pm 1}\Big[\mathcal{F}(-\gamma-\tilde{\epsilon}; 1-2\gamma; \rho) \mp \frac{-\gamma-\tilde{\epsilon}}{j+\tilde{m}}\mathcal{F}(1-s\gamma-\tilde{\epsilon}; 1-2s\gamma; \rho)\Big] \tag{11}$$

is defined in terms of confluent hypergeometric functions of the first kind. $\tilde{m} = mg/\beta$, $\tilde{\epsilon} = \epsilon g/\beta$ and $\rho = 2\beta r$ are the normalized mass, energy and distance away from the impurity. For $r \leq a$, the solution is defined in terms of Bessel functions

$$F_j^{-}(r) = J_{j-1/2}(\sqrt{E_+E_-}\,r) \tag{12}$$

and

$$F_j^{(+)}(r) = -\frac{1}{E_+}\left\{\partial_r[\sqrt{r}F_j^{(-)}(r)] - \frac{j}{r}\sqrt{r}F_j^{(-)}(r)\right\}, \tag{13}$$

where $E_\pm = \epsilon - V(a) \pm m$.

The energy of the levels follows from matching the wavefunctions at $r = a$, $\Psi_{r<a}(a) = \Psi_{r>a}(a)$, as shown in Fig. 2. For a given angular momentum state j, there is an infinite number of solutions that can be labeled by the index $n \in \mathbb{N}$, which is a non-negative integer. The lowest energy solution is labeled $n = 0$, with higher $n > 0$ attributed to the other higher excited states. For $j = \frac{1}{2}$ and $\epsilon = -m$, the critical coupling of the $n = 0$ level state is $g_c = 0.916$. The spectrum is in excellent agreement with the numerical results of [19].

Hubbard *U* term. The Coulomb interaction among electrons in the lowest energy state $n = 0$ and $j = \frac{1}{2}$ is described by

$$\mathcal{H}_C = \frac{1}{2}\int \mathrm{d}^2r\mathrm{d}^2r'\hat{\rho}(\mathbf{r})\frac{e^2}{\kappa|\mathbf{r}-\mathbf{r}'|}\hat{\rho}(\mathbf{r}'), \tag{14}$$

where $\hat{\rho}(\mathbf{r}) = \sum_\sigma \hat{\Theta}^\dagger_\sigma(\mathbf{r})\hat{\Theta}_\sigma(\mathbf{r})$ is the density operator defined in terms of the field operator $\hat{\Theta}_\sigma(\mathbf{r}) = \sum_\nu \Phi_{\frac{1}{2},\nu}(\mathbf{r})c_{\nu,\sigma}$. Hamiltonian (14) can be expressed explicitly in terms of c operators, resulting in the Hubbard U Hamiltonian described in the main text. The exchange term that also follows from (14) is identically zero due to the orthogonality of the two valley eigenspinors.

Spin-orbital exchange Hamiltonian. In second order of perturbation theory, the superexchange Hamiltonian is expressed in terms of c operators as:

$$\mathcal{H}_s = -J_s\sum_{\langle ij\rangle}\sum_{\{\nu\},\{\sigma\}} c^\dagger_{i,\nu,\sigma}c_{j,\nu,\sigma}c^\dagger_{j,\nu',\sigma'}c_{i,\nu',\sigma'}, \tag{15}$$

with $J_s = t^2/U$. The exchange interaction between NN sites can be calculated from the Coulomb interaction $\sum_{\langle ij\rangle}\mathcal{H}_{C,ij}$,

$$\mathcal{H}_{C,ij} = \frac{1}{2}\int \mathrm{d}^2r\mathrm{d}^2r'\hat{\rho}(\mathbf{r}_i)\frac{e^2}{\kappa|\mathbf{r}-\mathbf{r}'|}\hat{\rho}(\mathbf{r}'_j). \tag{16}$$

We extend the definition of the field operators as a sum over lattice sites, $\Theta_\sigma(\mathbf{r}) = \sum_{\nu,i}\Phi_{\frac{1}{2},\nu}(\mathbf{r}_i)c_{i,\nu\sigma}$. The exchange part of the interaction above term can be explicitly written as

$$\mathcal{H}_e = J_e\sum_{\langle ij\rangle}\sum_{\{\nu\}\{\sigma\}} c^\dagger_{i,\nu,\sigma}c^\dagger_{j,\nu',\sigma'}c_{i\nu',\sigma'}c_{j,\nu,\sigma}, \tag{17}$$

where J_e is given in the text. Hamiltonians (15) and (17) both map into pseudospin (valley) and spin operators, $\boldsymbol{\tau} = (\tau^x, \tau^y, \tau^z)$ and $\mathbf{S} = (S^x, S^y, S^z)$, through the following relations:

$$\begin{aligned}
c^\dagger_{i,\nu,\sigma}c_{i,\nu,\sigma} &\rightarrow \left(\frac{1}{2}+\nu\tau^z_i\right)\left(\frac{1}{2}+\sigma S^z_i\right)\\
c^\dagger_{i,\nu,\sigma}c_{i,-\nu,\sigma} &\rightarrow \tau^\nu\left(\frac{1}{2}+\sigma S^z_i\right)\\
c^\dagger_{i,\nu,\sigma}c_{i,\nu,-\sigma} &\rightarrow \left(\frac{1}{2}+\nu\tau^z_i\right)S^\sigma\\
c^\dagger_{i,\nu,\sigma}c_{i,-\nu,-\sigma} &\rightarrow \tau^\nu S^\sigma,
\end{aligned}$$

where $\tau^\nu = (\tau^x + \nu i\tau^y)$ and $S^\sigma = S^x + \sigma i S^y$. $\nu = \pm$, and $\sigma = \pm$ indexes the two valleys and spins respectively. This mapping results in Hamiltonian (9).

Acknowledgements

We are grateful to Kevin Beach, Frederic Mila and Kieran Mullen for numerous stimulating discussions. X. Dou and B. Uchoa acknowledge the University of Oklahoma for partial support. B. Uchoa was supported by NSF CAREER grant NMR-1352604. V. N. Kotov acknowledges support by the U.S. Department of Energy (DOE) grant DE-FG02-08ER46512. B. Uchoa thanks the Aspen Center of Physics where this work was partially completed.

Author contributions

X. D. did the analytical and numerical calculations. V. N. K. performed calculations and commented on the manuscript. B. U. coordinated the project, performed analytical calculations and wrote the manuscript.

Additional information

Competing financial interests: The authors declare no competing financial interests.

Correspondence

Correspondence and requests for materials should be addressed to B. U. (uchoa@ou.edu).

[1] Lee, P. A. An End to the Drought of Quantum Spin Liquids. Science **321**, 1306 (2008).

[2] Balents, L. Spin liquids in frustrated magnets. Nature **464**, 199–208 (2010).

[3] Kitaoka, Y. *et al.* Orbital frustration and resonating valence bond state in the spin-1/2 triangular lattice $LiNiO_2$. J. Phys. Soc. Jpn **67**, 3703 (1998).

[4] Mostovoy, M. V. & Khomskii, D. I. Orbital ordering in frustrated Jahn-Teller systems with 90° exchange. Phys. Rev. Lett. **89**, 227203 (2002).

[5] Reitsma, A. J. W., Feiner, L. F. & Oles, A. M. Orbital and spin physics in $LiNiO_2$ and $NaNiO_2$. New J. Phys. **7**, 121 (2005).

[6] Fritsch, V. *et al.* Spin and orbital frustration in $MnSc_2S_4$ and $FeSc_2S_4$. Phys. Rev. Lett. **92**, 116401 (2004).

[7] Vernay, F., Penc, K., Fazekas, P. & Mila, F. Orbital degeneracy as a source of frustration in $LiNiO_2$. Phys. Rev. B **70**, 014428 (2004).

[8] Bonda, M. *et al.* Effect of magnesium doping on the orbital and magnetic order in LiNiO2. Phys. Rev. B **78**, 104409 (2008).

[9] Fichtl, R., Lunkenheimer, P., Hemberger, J., Tsurkan, V. & Loidl, A. Glassy freezing of orbital dynamics in $FeCr_2S_4$ and $FeSc_2S_4$. J. Non-Cryst. Solids **351**, 2793–2797 (2005).

[10] Lewis, M. J. *et al.* Ordering and spin waves in NaNiO2: a stacked quantum ferromagnet, Phys. Rev. B **72**, 014408 (2005).

[11] Nakatsuji, S. *et al.* Spin-Orbital Short-Range Order on a Honeycomb-Based Lattice, Science **336**, 559 (2012).

[12] Ishiguro, Y. *et al.* Dynamical spin–orbital correlation in the frustrated magnet $Ba_3CuSb_2O_9$. Nat. Comm. **4**, 1 (2013).

[13] Li, Y. Q., Ma, M., Shi, D. N. & Zhang, F. C. SU(4) Theory for Spin Systems with Orbital Degeneracy. Phys. Rev. Lett. **81**, 3527 (1988).

[14] Gorshkov, A. V. *et al.* Two-orbital SU(N) magnetism with ultracold alkaline-earth atoms. Nat. Phys. **6**, 289 (2010).

[15] Zhang, X. *et al.* Spectroscopic observation of SU(N)-symmetric interactions in Sr orbital magnetism. Science **345**, 1467 (2014).

[16] Jördens, R., Strohmaier, N., Gunter, K., Moritz, H. & Esslinger, T. A. Mott insulator of fermionic atoms in an optical lattice. Nature **455**, 204 (2008).

[17] Cazalilla, M. A. & Rey, A. M. Ultracold Fermi gases with emergent SU(N) symmetry. Rep. Prog. Phys. **77**, 124401 (2014).

[18] Kugel, K. I., Khomskii, D. I., Sboychakov, A. O. & Streltsov, S. V. Spin-orbital interaction for face-sharing octahedra: Realization of a highly symmetric SU(4) model. Phys. Rev. B **91**, 155125 (2015).

[19] Pereira, V. M., Kotov, V. N. & Castro Neto, A. H. Supercritical Coulomb impurities in gapped graphene. Phys. Rev. B **78**, 085101 (2008).

[20] Novikov, D. S. Elastic scattering theory and transport in graphene. Phys. Rev. B **76**, 245435 (2007).

[21] Kotov, V. N., Uchoa, B., Pereira, V. M., Guinea, F. & Castro Neto. A. H. Electron-electron interactions in graphene: current status and perspectives. Rev. Mod. Phys. **84**, 1067 (2012).

[22] Goerbig, M. O. Electronic properties of graphene in a strong magnetic field. Rev. Mod. Phys. **83**, 1193 (2011).

[23] Young, A. F. *et al.* Spin and valley quantum Hall ferromagnetism in graphene. Nature Phys. **8**, 550 (2012).

[24] Young, A. F. *et al.* Tunable symmetry breaking and helical edge transport in a graphene quantum spin Hall state. Nature **505**, 528 (2013).

[25] Nomura, K. & McDonald, A. H. Quantum Hall ferromagnetism in graphene. Phys. Rev. Lett. **96**, 256602 (2006).

[26] Alicea, J. & Fisher, M. P. A. Graphene integer quantum Hall effect in the ferromagnetic and paramagnetic regimes. Phys. Rev. B **74**, 075422 (2006).

[27] Abanin, D. A., Feldman, B. E., Yacoby, A. & Halperin, B. I. Fractional and integer quantum Hall effects in the zeroth Landau level in graphene. Phys. Rev. B **88**, 115407 (2013).

[28] Sodemann, I. & MacDonald, A. H. Broken SU(4) Symmetry and The Fractional Quantum Hall Effect in Graphene. Phys. Rev. Lett. **112** 126804 (2014).

[29] Zhou, S. Y. *et al.* Substrate-induced bandgap opening in epitaxial graphene. Nature Mater. **6**, 770 (2007).

[30] Nevius, M. S. *et al.* Semiconducting graphene from highly ordered substrate interactions. Phys. Rev. Lett. **115**, 136802 (2015).

[31] Corboz, P., Lajko, M., Lauchli, A. M., Penc, K. & Mila, F. Spin-Orbital Quantum Liquid on the Honeycomb Lattice. Phys. Rev. X **2**, 041013 (2012).

[32] Penc, K., Mambrini, M., Fazekas, P. & Mila, F. Quantum phase transition in the SU(4) spin-orbital model on the triangular lattice. Phys. Rev. B **68**, 012408 (2003).

[33] Corboz, P., Lauchli, A. M., Penc, K., Troyer, M. & Mila, F. Simultaneous dimerization and SU(4) symmetry breaking of 4-color fermions on the square lattice. Phys. Rev. Lett. **107**, 215301 (2011).

[34] Wang, F. & Vishwanath, A. Z_2 spin-orbital liquid state in the square lattice Kugel-Khomskii model. Phys. Rev. B **80**, 064413 (2009).

[35] Reinhardt, J. & Greiner, W. Quantum electrodynamics of strong fields. Rep. Prog. Phys. **40**, 219 (1977).

[36] Zeldovich, Y. B. & Popov, V. S. Electronic structure of superheavy atoms. Sov. Phys. Usp. **14**, 673 (1972).

[37] Kugel, K. I. & Khomskii, D. I. Crystal structure and magnetic properties of substances with orbital degeneracies. Sov. Phys. Usp. **25**, 231 (1982).

[38] Eigler, D. M. & Schweizer, E. K. Positioning single atoms with a scanning tunnelling microscope. Nature **344**, 524 (1990).

[39] Mak, K. F., Lee, C., Hone, J., Shan, J. & Heinz, T. F. Atomically Thin MoS2: A New Direct-Gap Semiconductor. Phys. Rev. Lett. **105**, 136805 (2010).

[40] Zhu, Z. Y., Cheng, Y. C. & Schwingenschlögl, U. Gi-

ant spin-orbit-induced spin splitting in two-dimensional transition-metal dichalcogenide semiconductors. Phys. Rev. B **84**, 153402 (2011).

[41] Caragiu, M. & Finberg, S. Alkali metal adsorption on graphite: a review. J. Phys. Condens. Matter **17**, R995 (2005).

[42] Brar, V. W. *et al.* Gate-controlled ionization and screening of cobalt adatoms on a graphene surface. Nat. Phys. **7**, 43 (2011).

[43] Hermele, M., Senthil, T. & Fisher, M. P. A. Algebraic spin liquid as the mother of many competing orders, Phys. Rev. B **72**, 104404 (2005).

[44] Marston, B. & Affleck, I. Large-n limit of the Heisenberg-Hubbard model: Implications for high-T_c superconductors, Phys. Rev. B **37**, 3774 (1988).

[45] Chatterjee, S. & Sachdev, S. Probing excitations in insulators via injection of spin currents. Phys. Rev. B **92**, 165113 (2015).

[46] Chen, C.-Z., Sun, Q., Wang, F. & Xie, X. C. Detection of spinons via spin transport. Phys. Rev. B **88**, 041405(R) (2013).

[47] Hung, H.-H., Yang, Y. & Wu, C. Quantum magnetism in ultracold alkali and alkaline-earth fermion systems with symplectic symmetry. Phys. Rev. B **84**, 054406 (2011).

[48] Fu, M., Imai, T., Han, T. -H. & Lee, Y. S. Evidence for a gapped spin-liquid ground state in a kagome Heisenberg antiferromagnet. Science **350,** 655 (2015).

[49] Uchoa, B., Kotov, V. N. & Kindermann, M. Valley order and loop currents in graphene on hexagonal boron nitride, Phys. Rev. B **91**, 121412(R) (2015).

arXiv:1602.01477v2 [cond-mat.mes-hall] 30 Aug 2016

Suplementary Materials of "Designing Quantum Spin-Orbital Liquids in Artificial Mott Insulators"

Xu Dou,[1] Valeri N. Kotov,[2] and Bruno Uchoa[1,*]

[1]*Department of Physics and Astronomy, University of Oklahoma, Norman, OK 73069, USA*
[2]*Department of Physics, University of Vermont, Burlington, VT 05405, USA*

Wavefunction of the strong coupling subcritical regime

The wave function $\Psi(\mathbf{r})$ of a two dimensional massive Dirac fermion moving around a Coulomb impurity satisfies,

$$(-i\boldsymbol{\sigma}\cdot\boldsymbol{\nabla}+V(r)+m\sigma_z)\Psi(\mathbf{r})=\epsilon\Psi(\mathbf{r}), \tag{1}$$

where

$$V(r)=\begin{cases}-g/r, & r>a\\ -g/a, & r\leq a\end{cases}$$

is the regularized Coulomb potential. Here we set $\hbar=v=1$.

The two-component wave function is

$$\Psi(r,\phi)=\frac{1}{\sqrt{2\pi}}\begin{pmatrix}F_j^{(-)}(r)e^{i(j-1/2)\phi}\\ F_j^{(+)}(r)e^{i(j+1/2)\phi}\end{pmatrix}, \tag{2}$$

he Dirac equation with the presence of an external potential becomes

$$\begin{bmatrix}\epsilon-m-U & -(\partial_r+\frac{\kappa+1}{r})\\ (\partial_r-\frac{\kappa}{r}) & \epsilon+m-U\end{bmatrix}\begin{pmatrix}F_j^{(-)}(r)\\ F_j^{(+)}(r)\end{pmatrix}=0$$

or equivalently

$$\begin{aligned}\frac{dF_j^{(-)}}{dr}-\frac{\kappa}{r}F_j^{(-)}+(\epsilon+m-U)F_j^{(+)}&=0\\ \frac{dF_j^{(+)}}{dr}+\frac{\kappa+1}{r}F_j^{(+)}-(\epsilon-m-U)F_j^{(-)}&=0\end{aligned} \tag{3}$$

where $\kappa=j-\frac{1}{2}$.

Solution for $r>a$

The wave functions assumes the form (j indexes will be dropped)

$$F^{(-)}(\rho)=\sqrt{m+\epsilon}e^{-\rho/2}\rho^{\gamma-1/2}(Q_1+Q_2)$$

$$F^{(+)}(\rho)=\sqrt{m-\epsilon}e^{-\rho/2}\rho^{\gamma-1/2}(Q_1-Q_2). \tag{4}$$

where $\rho=2\lambda r$, $\beta=\sqrt{m^2-\epsilon^2}$, and$\gamma=\sqrt{j^2-g^2}$. After some algebra, we get

$$\rho Q_1'+(\gamma-\frac{\epsilon g}{\beta})Q_1-(j+\frac{mg}{\beta})Q_2=0 \tag{5}$$

$$\rho Q_2'+(\gamma+\frac{\epsilon g}{\beta}-\rho)Q_2-(j-\frac{mg}{\beta})Q_1=0. \tag{6}$$

These equations can be decoupled

$$\rho Q_1'' + (1 + 2\gamma - \rho)Q_1' - (\gamma - \frac{\epsilon g}{\beta})Q_1 = 0$$

$$\rho Q_2'' + (1 + 2\gamma - \rho)Q_2' - (1 + \gamma - \frac{\epsilon g}{\beta})Q_2 = 0,$$

both of which are Kummer's differential equation

$$xy'' + (c - x)y' - ay = 0$$

with the solution $y = c\mathcal{F}(a; c; x)$. Here we call the confluent Hypergeometric function of the first kind ${}_1F_1(a; c; x)$ as $\mathcal{F}(a; c; x)$,

$${}_1F_1(a; c; x) = 1 + \frac{a}{c}x + \frac{a(a+1)}{c(c+1)}\frac{x^2}{2!} + ...,$$

and notice that ${}_1F_1(a; c; x = 0) = 1$. The solutions are

$$Q_1 = c_1\mathcal{F}(\gamma - \frac{\epsilon g}{\beta}; 1 + 2\gamma; \rho) + d_1\mathcal{F}(-\gamma - \frac{\epsilon g}{\beta}; 1 - 2\gamma; \rho) \tag{7}$$

$$Q_2 = c_2\mathcal{F}(1 + \gamma - \frac{\epsilon g}{\beta}; 1 + 2\gamma; \rho) + d_2\mathcal{F}(1 - \gamma - \frac{\epsilon g}{\beta}; 1 - 2\gamma; \rho). \tag{8}$$

Weak coupling regime

When $g < j$, γ is real. Integrability of the wavefunction at $\rho \to \infty$ requires that $d_1 = d_2 = 0$. From Eq.(5), one can determine the ratio

$$\frac{c_1}{c_2} = \frac{Q_1}{Q_2}\bigg|_{\rho=0} = \frac{j + \frac{mg}{\beta}}{\gamma - \frac{\epsilon g}{\beta}}.$$

To simplify the notation we call $\tilde{m} = mg/\beta$, $\tilde{\epsilon} = \epsilon g/\beta$, and

$$c_1 = c,\ c_2 = \frac{\gamma - \tilde{\epsilon}}{j + \tilde{m}}c.$$

That leads to the solution

$$F_j^{(-)}(\rho) = c\sqrt{m + \epsilon}e^{-\rho/2}\rho^{\gamma - 1/2}[\mathcal{F}(\gamma - \tilde{\epsilon}; 1 + 2\gamma; \rho) + \frac{\gamma - \tilde{\epsilon}}{j + \tilde{m}}\mathcal{F}(1 + \gamma - \tilde{\epsilon}; 1 + 2\gamma; \rho)]$$

$$F_j^{(+)}(\rho) = c\sqrt{m - \epsilon}e^{-\rho/2}\rho^{\gamma - 1/2}[\mathcal{F}(\gamma - \tilde{\epsilon}; 1 + 2\gamma; \rho) - \frac{\gamma - \tilde{\epsilon}}{j + \tilde{m}}\mathcal{F}(1 + \gamma - \tilde{\epsilon}; 1 + 2\gamma; \rho)]$$

This solution is regular at $\rho \to 0$, and the short distance cut-off can be set to zero.

Strong coupling regime

When the coupling $g > \frac{1}{2}$, γ becomes imaginary. With the requirement of imposing a small distance cut-off, the condition that the wave function behaves well at $\rho = 0$ is not necessary, so we should include both $\pm\gamma$ branches into the solutions. The ratio between the two And in this case we hope the wave functions die off at $\rho \to +\infty$, which

can also serve to settle down the ratio between $\gamma-$branch and $(-\gamma)$-branch. The formula can be used here is the asymptotic form of the hypergeometric function,

$$ {}_1F_1(a;b;x) \sim \Gamma(b)\left(\frac{e^z z^{a-b}}{\Gamma(a)} + \frac{(-z)^{-a}}{\Gamma(b-a)}\right). $$

The second part is required if the gamma function $\Gamma(a)$ is infinite (when a is a negative integer) or $\mathrm{Re}(z)$ is non-positive. In our case, we could exclude these two conditions, and only keep the second term. Therefore for large $|z|$, the dominating part (which is growing) of $\mathcal{F}(z)$ is

$$ \mathcal{F}(a;b;z) \sim \frac{\Gamma(b)}{\Gamma(a)} e^z z^{a-b}, $$

and we ask for some condition to cancel this term. For $aF(\rho;\gamma) + bF(\rho;-\gamma)$ we need the following two terms to be finite at $\rho \to +\infty$

$$ a\rho^{\gamma-1/2}\mathcal{F}(\gamma-\tilde{\epsilon};1+2\gamma;\rho) + b\rho^{-\gamma-1/2}\mathcal{F}(-\gamma-\tilde{\epsilon};1-2\gamma;\rho) \tag{9} $$

$$ a\rho^{\gamma-1/2}\frac{\gamma-\tilde{\epsilon}}{j+\tilde{m}}\mathcal{F}(1+\gamma-\tilde{\epsilon};1+2\gamma;\rho) + b\rho^{-\gamma-1/2}\frac{-\gamma-\tilde{\epsilon}}{j+\tilde{m}}\mathcal{F}(1-\gamma-\tilde{\epsilon};1-2\gamma;\rho) \tag{10} $$

From 9,

$$ \frac{a}{b} = -\frac{\Gamma(\gamma-\tilde{\epsilon})}{\Gamma(1+2\gamma)}\frac{\Gamma(1-2\gamma)}{\Gamma(-\gamma-\tilde{\epsilon})} = -\frac{\Gamma(\gamma-\tilde{\epsilon})}{(2\gamma)\Gamma(2\gamma)}\frac{(-2\gamma)\Gamma(-2\gamma)}{\Gamma(-\gamma-\tilde{\epsilon})} = \frac{\Gamma(\gamma-\tilde{\epsilon})}{\Gamma(2\gamma)}\frac{\Gamma(-2\gamma)}{\Gamma(-\gamma-\tilde{\epsilon})}. $$

We can assign

$$ a = \frac{\Gamma(-2\gamma)}{\Gamma(-\gamma-\tilde{\epsilon})}, \qquad b = \frac{\Gamma(2\gamma)}{\Gamma(\gamma-\tilde{\epsilon})} \tag{11} $$

The solution for $F^{(\pm)}$ is

$$ \begin{aligned} F_j^{(\mp)}(r) = {} & c'\sqrt{m\pm\epsilon}e^{-\rho/2}\rho^{-1/2} \\ & \times\left[\frac{\Gamma(-2\gamma)}{\Gamma(-\gamma-\tilde{\epsilon})}\rho^{\gamma}\mathcal{F}(\gamma-\tilde{\epsilon};1+2\gamma;\rho) + \frac{\Gamma(2\gamma)}{\Gamma(\gamma-\tilde{\epsilon})}\rho^{-\gamma}\mathcal{F}(-\gamma-\tilde{\epsilon};1-2\gamma;\rho)\right. \\ & \left.\pm\frac{\Gamma(-2\gamma)}{\Gamma(-\gamma-\tilde{\epsilon})}\frac{\gamma-\tilde{\epsilon}}{j+\tilde{m}}\rho^{\gamma}\mathcal{F}(1+\gamma-\tilde{\epsilon};1+2\gamma;\rho) \pm \frac{\Gamma(2\gamma)}{\Gamma(\gamma-\tilde{\epsilon})}\frac{-\gamma-\tilde{\epsilon}}{j+\tilde{m}}\rho^{-\gamma}\mathcal{F}(1-\gamma-\tilde{\epsilon};1-2\gamma;\rho)\right] \end{aligned} \tag{12} $$

Solution for $r \le a$

In the $r < a$ region, we define

$$ F_j^{(-)}(r) = \frac{1}{\sqrt{r}}A(r) $$
$$ F_j^{(+)}(r) = \frac{1}{\sqrt{r}}B(r) $$

the Dirac equation becomes

$$ A'(r) - \frac{j}{r}A(r) + E_+B(r) = 0 $$

$$ B'(r) + \frac{j}{r}B(r) - E_-A(r) = 0 $$

where $E_\pm = \epsilon + \frac{g}{a} \pm m$. These equations can be decoupled into

$$A''(r) + (E_+E_- + \frac{j-j^2}{r^2})A(r) = 0$$

$$B''(r) + (E_+E_- - \frac{j+j^2}{r^2})B(r) = 0$$

The solutions are

$$A(r) = c_1\sqrt{r}J_{j-1/2}(\sqrt{E_+E_-}r)$$

$$B(r) = c_2\sqrt{r}J_{j+1/2}(\sqrt{E_+E_-}r)$$

and $\sqrt{E_+E_-} = \sqrt{\epsilon^2 + (g/a)^2 + (2\epsilon g/a) - m^2}$.

From

$$B(r) = -\frac{A' - \frac{j}{r}A}{E_+},$$

we have

$$B(r) = -\frac{c_1}{E_+}[\frac{\frac{1}{2}-j}{\sqrt{r}}J_{j-1/2}(\sqrt{E_+E_-}r) + \sqrt{r}J'_{j-1/2}(\sqrt{E_+E_-}r)]$$

Energy

The energy ϵ can be determined by matching the inside solution and the outside one, formally through

$$Out(j,\epsilon,r,g)\big|_{r=a} = Ins(j,\epsilon,r,g)\big|_{r=a}$$

For given j, g, and at $r = a$, we can determine the energy ϵ

$$\left(\begin{array}{c}\sqrt{r}F(r)\\ \sqrt{r}G(r)\end{array}\right)\Big|_{r=a} = \left(\begin{array}{c}A(r)\\ B(r)\end{array}\right)\Big|_{r=a}$$

* Electronic address: uchoa@ou.edu

[1] D.S. Novikov, Phys. Rev. B 76, 245435 (2007).
[2] V.M. Pereira, V.N. Kotov, and A.H. Castro Neto, Phys. Rev. B 78, 085101 (2008)